Drift of Levitated/Suspended Body in High-T_c Superconducting Levitation Systems Under Vibration—Part I: A Criterion Based on Magnetic Force-Gap Relation for Gap Varying With Time

Xiao-Fan Gou, Xiao-Jing Zheng, and You-He Zhou

***Abstract*—Levitation drift in the high-T_c superconducting levitation systems is directly related to the safe operation of the systems. In these levitation systems, the gap between a superconductor and a permanent magnet may decrease, increase, or keep unvarying with time. Based on the numerical simulations of the magnetic force-gap hysteresis relations of two different physical processes in field cooling, and the dynamic features at some given positions on major magnetic force-gap loops, a criterion described by the slopes of the given position on minor and major loops is proposed in this study. According to the suggested criterion, the drift phenomenon can be characterized by judging gap varying with time for a given levitation system. In addition, the characteristic of continuous space range of the equilibrium position of levitated/suspended body has been further exhibited from the numerical results.**

***Index Terms*—Criterion, drift, high-T_c superconducting levitation system, magnetic force-gap relation.**

I. Introduction

THE high-T_c superconducting levitation is based on the interaction between a magnet and a high-T_c superconductor (HTSC). Due to its unique characteristics [1], [2], it has demonstrated tremendous potential for several fascinating applications such as the magnetic levitation [3]–[5], the noncontact transport, and the flywheel energy storage, etc. [6], [7]. In connection with these applications, it is very important to study the stability of the main levitation parameters: load capacity, stiffness, gap between a superconductor and a permanent magnet (PM). Some experiments have found that, even for a very simple levitation system (a PM is levitated above an HTSC, or suspended below an HTSC), a vibration of PM/HTSC or an alternating magnetic field applied to an HTSC can make the levitated body (LB) drift (i.e., gap varying with time) [8]–[10] or even collapse [11], which is directly related to the safe operation and design of the whole system.

Nemoshkalenko *et al.* [8] and Terentiev *et al.* [9] first observed that the drift vertically down (i.e., gap decreasing with time) from the LB is induced by a vibration of HTSC/PM or an alternating magnetic field applied to an HTSC. Using various HTSC samples such as free-sintered, melt-quenched, and melt-powder-melt-growth ones, Hikihara *et al.* [10] found that the drift does not depend on the preparation method of HTSC, material, and the cooling method, but mainly on the hysteresis relation between magnetic force and gap. Furthermore, Coombs *et al.* [11] further suggested that, during the vibration of LB, there exists not only the possibility of the gap decreasing (levitation case), but also that of the gap increasing (suspension case), which depends on the position of operation point on major magnetic force-gap loops. Recently, Zheng *et al.* [12] have studied the influence of flux creep on dynamic behavior of the levitation system numerically, in which the flux creep is considered as one of the main reasons for the time decay of the levitation properties, namely, the magnetic forces and levitation/suspension gaps. For a better understanding of the levitation drift, it is very necessary to further investigate the problem from the theoretical, especially quantitative, aspect.

The aim of this series of papers is to study drift of LB/suspended body (SB) in high-T_c superconducting levitation systems under vibration numerically. In the first paper of this series, the rule of levitation/suspension gap varying with time is explored, and the corresponding criterion is also proposed. Moreover, the equilibrium position of the LB/SB for a given high-T_c superconducting levitation system is a continuous range rather than a space point, which has even been studied by Brandt [13] and by Navau *et al.* [14] from the static aspect. In this paper, the unique characteristic will be further investigated from the dynamic aspect.

II. Basic Equations

The essential equations of the superconductor-PM levitation system are introduced in this section. As shown in Fig. 1, an axisymmetric high-T_c superconducting levitation system is mainly made up of two parts: a cylindrical HTSC and a PM in connection with/without an additional load. In general, by means of adjusting the weight of the additional load, we can realize the given levitation height (gap) of the LB. So, the LB moves coaxially over the superconductor subjected to a vertical excitation.

Manuscript received February 9, 2006; revised November 10, 2006. This work was supported by the Fund of Pre-Research for Key Basic Researches of the Ministry of Science and Technology of China, by the Fund of the National Science Foundation of China (10472038), by the doctoral fund of the Ministry of Education of China (20050730016), by the Youth Fund of the National Science Foundation of China (10502019), China Postdoctoral Science Foundation, and by the Postdoctoral Research Project of Jiangsu Province. This paper was recommended by Associate Editor P. J. Masson.

X.-F. Gou is with the Department of Engineering Mechanics, Hohai University, Nanjing, Jiangsu 210098, China (e-mail: xfgou@163.com).

X.-J. Zheng and Y.-H Zhou are with the Department of Mechanics, Lanzhou University, Lanzhou, Gansu 730000, China (e-mail: xjzheng@lzu.edu.cn; zhouyh@lzu.edu.cn).

Digital Object Identifier 10.1109/TASC.2007.902104

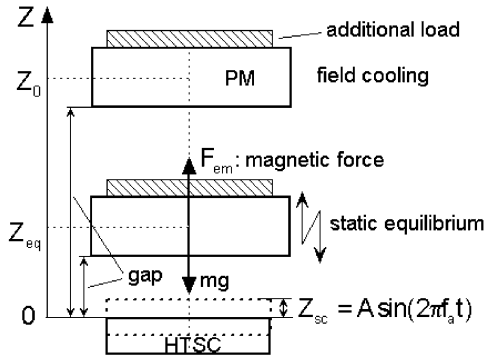

Fig. 1. Schematic drawing of an HTSC-PM levitation system subjected to an external excitation.

Besides the gravity force, a magnetic force acting on the PM is arising from the interaction between the PM and the superconductor, which is given by

$$\mathbf{F}_{\rm em} = \int_V \mathbf{J} \times \mathbf{B}_{\rm ex} dV \tag{1}$$

where V represents the volume of the superconductor; $\mathbf{J}$ is the shielding current density; and $\mathbf{B}_{\rm ex}$ is the external magnetic induction from the PM. Having introduced the magnetic vector potential $\mathbf{A}$ to the PM, we can express $\mathbf{B}_{\rm ex}$ by [15]

$$\mathbf{B}_{\rm ex}(\rho, Z) = \nabla \times \mathbf{A} = -\frac{\partial A_\phi}{\partial Z}\mathbf{e}_\rho + \frac{1}{\rho}\frac{\partial}{\partial \rho}(\rho A_\phi)\mathbf{e}_z \tag{2}$$

where $A_\phi(\rho, Z) = \mu_0 aI/(4\pi)\int_0^{2\pi} (\cos\phi'/\sqrt{a^2+\rho^2-2a\rho\cos\phi'+Z^2})d\phi$; ρ and ϕ are the radial and circumferential coordinates, respectively; Z is a longitudinal coordinate away from the center of the magnet surface for a field point (ρ, ϕ, Z) (see Fig. 1); a is the radius of the cross section of the PM; and I is the nominal current strength usually determined by the residual magnetic field of the PM.

From the macroscopic view, the shielding current density $\mathbf{J}$, the magnetic induction $\mathbf{B}$, and the electric field intensity $\mathbf{E}$ should satisfy the Maxwell equations, i.e.,

$$\nabla \times \mathbf{H} = \mathbf{J}, \quad \nabla \times \mathbf{E} = -\frac{\partial \mathbf{B}}{\partial t} \tag{3}$$

where $\mathbf{B} = \mathbf{B}_{\rm ex} + \mathbf{B}_{\rm sc}$, in which $\mathbf{B}_{\rm sc}$ is the induced part of $\mathbf{B}$ due to the shielding current in the superconductor. And the quasi-static law of electric charge conservation as neglecting the term $\partial\rho/\partial t$

$$\nabla \cdot \mathbf{J} = 0 \tag{4}$$

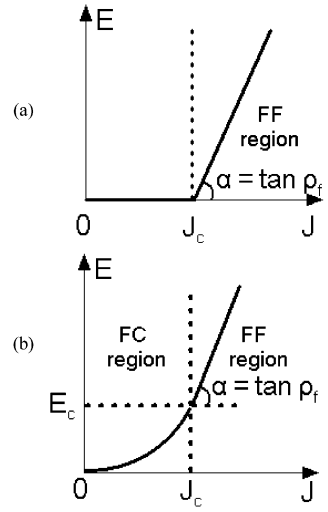

Fig. 2. Diagram of macro-models of HTSCs employed recently. (a) Flux flow model; (b) flux flow and creep model.

where ∇ is the gradient operator; $\mathbf{H} = (1/\mu_0)\mathbf{B}$ indicates the magnetic field vector in the superconductor, and μ_0 is the magnetic permeability in vacuum.

To the HTSC, a general form of constitutive relation linking the electric field intensity $\mathbf{E}$ and the current density $\mathbf{J}$ can be written by [16]

$$\mathbf{E} = f(|\mathbf{J}|)\frac{\mathbf{J}}{|\mathbf{J}|}. \tag{5}$$

Here, $f(\cdot)$ is a prespecific function dependent on what superconductor features are taken into account in a macro-model of HTSCs. For the flux flow model of the HTSCs, for example, we have [17], [18]

$$f(|\mathbf{J}|) = E = \begin{cases} 0, & 0 \leqslant |\mathbf{J}| \leqslant J_c \\ \rho_f J_c\left(\frac{|\mathbf{J}|}{J_c} - 1\right), & |\mathbf{J}| > J_c \end{cases} \tag{6}$$

and for the flux flow and creep model, the constitutive relation is formulated by (7), shown at the bottom of the page [16], [19], where, $E_c = \rho_c J_c\{1 - \exp(-2U_0/k\theta)\} \approx \rho_c J_c$; ρ_c represents the creep resistivity; J_c is the critical current density without thermal activation; U_0 stands for the pinning potential; k indicates the Boltzmann constant; θ is the absolute temperature; and ρ_f denotes the flow resistivity. These two constitutive relations are schematically shown in Fig. 2, in which both the flux flow and creep phenomena are considered only in the flux flow and creep model, whereas the flux creep phenomenon is neglected in the flux flow model.

Due to nonlinearity of each constitutive relation between electric field $\mathbf{E}$ and current density $\mathbf{J}$, the electromagnetism of

$$f(|\mathbf{J}|) = E = \begin{cases} 2\rho_c J_c \sinh\left(\frac{U_0}{k\theta}\frac{|\mathbf{J}|}{J_c}\right)\exp\left(-\frac{U_0}{k\theta}\right), & 0 \leqslant |\mathbf{J}| \leqslant J_c \\ E_c + \rho_f J_c\left(\frac{|\mathbf{J}|}{J_c} - 1\right), & |\mathbf{J}| > J_c \end{cases} \tag{7}$$

HTSCs is nonlinear too, i.e., the governing (2)–(5) associated with either (6) or (7) are nonlinear. In this case, it is obvious that the electromagnetic fields in the superconductor are dependent on spanning distance (or gap) and speed of movement between the superconductor and the PM. Denote the spanning distance by $Z = Z(t)$. The magnetic force changes with the spanning distance and its velocity except for the distribution of magnetic field of PM and superconductor parameters. Thus, we can formulate this dependency by a function $\mathbf{F}_{\rm em} = \mathbf{F}_{\rm em}(Z, \dot{Z})$ mathematically.

In order to determine the unknown function $Z = Z(t)$, we have to study the vertical movement of the LB. Here, we consider that superconductor is cooled down below the critical temperature T_c for a sufficient critical current. Then the PM slowly moved from an initial position Z_0 to a static equilibrium position $Z_{\rm eq}$ ($F_{\rm em} - mg = 0$). Denote $z = Z - Z_{\rm eq}$. From Newton's second law, the dynamic equation of vertical movement of the PM can be expressed as

$$m\ddot{z} + c\dot{z} - F_{\rm em} + mg = F_a(t) \tag{8}$$

and the initial conditions are taken into account by

$$t = 0: \quad z = z_0, \dot{z} = \dot{z}_0. \tag{9}$$

Here, m is the mass of the LB, c stands for the air-damping coefficient, and g is the gravitational acceleration; z, $\dot{z}$, and $\ddot{z}$ are, respectively, the displacement, velocity, and acceleration of the PM relative to its static equilibrium position; $F_{\rm em}$ represents the vertical component of magnetic force $\mathbf{F}_{\rm em}$; $F_a(t)$ indicates an external excitation force. When an external excitation $Z_{\rm sc}$ of displacement is applied to the superconductor, for example, we have $F_a(t) = -m\ddot{Z}_{\rm sc} - c\dot{Z}_{\rm sc}$.

III. Numerical Procedure

Up to now, almost no analytical solution has been found to solve a problem of macro-electromagnetism of superconductors with finite geometric scale even if they have a simple geometric shape. In this paper, we pay attention to the establishment of a numerical code to solve the nonlinear and coupled problem of the superconductor-PM levitation systems. Here, the T-method of eddy or shielding current and the finite element method (FEM) for electromagnetic fields of superconductors are employed, and some iteration approaches are chosen to solve the nonlinearity and coupling. For example, a direct iteration is employed to the nonlinear differential equation (8) by the form

$$m\ddot{z}^{(i+1)} + c\dot{z}^{(i+1)} - F_{\rm em}^{(i)} + mg = F_a(t). \tag{10}$$

Here, the superscript $i (i = 1, 2, \ldots)$ indicates the number of iteration step, and

$$F_{\rm em}^{(i)}\mathbf{e}_z = \int_V \mathbf{J}^{(i)} \times \mathbf{B}_{\rm ex}^{(i)} dV. \tag{11}$$

The main steps of the numerical code are briefly introduced as follows:

Step 1) Input the iterating values of $z(t)$ and $\dot{z}(t)$, i.e., $z^{(i)}(t)$ and $\dot{z}^{(i)}(t)$. At the first step or $i = 1$, they are taken as their initial values of (9).

Step 2) Perform calculation of electromagnetic fields at ith step.

1) *T-method*. According to the quasi-static law of electric charge conservation of (4), the current vector potential $\mathbf{T}$ (satisfies $\nabla \times \mathbf{T} = \mathbf{J}$) is introduced. Due to the axial symmetry, the current density can be expressed by the vector $\mathbf{T}$ in axial coordinates (ρ, φ, z) as

$$\mathbf{J}(\rho, z) = \left(\frac{\partial T_\rho}{\partial z} - \frac{\partial T_z}{\partial \rho}\right)\mathbf{e}_\varphi. \tag{12}$$

For a disk-shape anisotropic superconductor, considering thin plate assumption [20], the current density along thickness direction keeps unvaried, i.e., is independent of z. Accordingly, the current vector potential $\mathbf{T}$ has only a normal component $T_z(\rho)\mathbf{e}_z$. In this case, the governing (3) of electromagnetic fields of superconductors can be rewritten as

$$\nabla \times \frac{1}{\sigma_s}(\nabla \times \mathbf{T}^{(i)}) = -\frac{\partial(\mathbf{B}_{\rm sc}^{(i)} + \mathbf{B}_{\rm ex}^{(i)})}{\partial t} \tag{13}$$

which is the governing equation for the unknown function of current potential at the ith step. In (13), σ_s is an effective conductivity of the superconductor following Ohm's law $\mathbf{J} = \sigma_s \mathbf{E}$. Applying Helmholtz's formula to the induced magnetic induction in the superconductor, we get an integral equation of the induced magnetic induction $\mathbf{B}_{\rm sc}^{(i)}$ as follows [20]:

$$\mathbf{B}_{\rm sc}^{(i)} = \mu_0 \mathbf{T}^{(i)} + \frac{\mu_0}{4\pi}\int_S (\mathbf{T}^{(i)} \bullet \mathbf{n})\nabla' \frac{1}{R} dS \tag{14}$$

where $\mathbf{n}$ is the unit vector normal to the surface of the superconductor, and R indicates the distance between a source point and a field one. Substituting (14) into (13), we obtain the governing equation for $\mathbf{T}^{(i)}$ of the form

$$\nabla \times \frac{1}{\sigma_s}\nabla \times \mathbf{T}^{(i)} + \mu_0 \frac{\partial \mathbf{T}^{(i)}}{\partial t} + \frac{\mu_0}{4\pi}\int_S \frac{\partial(\mathbf{T}^{(i)} \bullet \mathbf{n})}{\partial t}\nabla' \frac{1}{R} dS + \frac{\partial \mathbf{B}_{\rm ex}^{(i)}}{\partial t} = \mathbf{0} \tag{15}$$

or

$$\mathbf{n} \bullet \nabla \times \frac{1}{\sigma_s}\nabla \times (T^{(i)}\mathbf{n}) + \mu_0 \frac{\partial T^{(i)}}{\partial t} + \frac{\mu_0}{4\pi}\mathbf{n} \bullet \int_S \frac{\partial T^{(i)}}{\partial t}\nabla' \frac{1}{R} dS + \frac{\partial B_{\rm ex}^{(i)}}{\partial t} = 0. \tag{16}$$

Here, $B_{\rm ex}^{(i)}$ is the normal component of $\mathbf{B}_{\rm ex}^{(i)}$.

2) *FEM*. After the boundary conditions for unknown function $T = T(\rho, t)$ is taken into account in the differential equation (16), the FEM can be used to get a numerical solution of the equation, to which the system of algebraic equations can be compactly expressed by the following matrix form [21]:

$$[\mathbf{A}][\dot{\mathbf{T}}^{(i)}] + [\mathbf{C}][\mathbf{T}^{(i)}] = [\dot{\mathbf{B}}_{\rm ex}]. \tag{17}$$

TABLE I
GEOMETRICAL AND PHYSICAL PARAMETERS EMPLOYED IN SIMULATION

	Diameter (mm)	Thick (mm)	J_c (A/m^2)	E_c (V/m)	U_0 (eV)	ρ_f (Ωm)	Residual field (Tesla)
HTSC	18	2.5	5.0×10^{7}	1.0×10^{-4}	0.1	5.0×10^{-10}	
PM	25	22.5					0.4

TABLE II
GEOMETRICAL AND PHYSICAL PARAMETERS EMPLOYED IN EXAMINATION 2

	Diameter (mm)	Thick (mm)	J_c (A/m^2)	E_c (V/m)	U_0 (eV)	ρ_f (Ωm)	Residual field (Tesla)
HTSC	1.2	1.2	1.0×10^{6}	1.0×10^{-6}	0.1	5.0×10^{-10}	
PM	17/34	10					0.06

Here, $[\mathbf{A}]$ and $[\mathbf{C}]$ are the square matrices of coefficients and they are respectively relative to those coefficients of terms $\partial T^{(i)}/\partial t$ and $T^{(i)}$ in (16); $[\mathbf{T}^{(i)}]$ indicates the column matrix of unknown function $T^{(i)}$; $[\dot{\mathbf{T}}^{(i)}]$ means the column matrix of differentiation of $[\mathbf{T}^{(i)}]$ with respect to time variable; and $[\dot{\mathbf{B}}_{\rm ex}]$ represents the column matrix of excitation related to the last term of (16). It is evident that the matrix $[\mathbf{C}]$ is dependent upon the equivalent conductivity, i.e., $[\mathbf{C}] = [\mathbf{C}(\sigma_s)]$. According to the definition of conductivity, we know that the effective conductivity σ_s to the superconductor is piecewise dependent on both electric field intensity $\mathbf{E}$ and shielding current density $\mathbf{J}$. Thus, the matrix equation of (17) is nonlinearly dependent on the unknown column $[\mathbf{T}^{(i)}]$.

3) *Iteration approach*. To the nonlinear equation (17) of electromagnetic fields, another iteration is taken as

$$[\mathbf{A}]\left[\dot{\mathbf{T}}^{(i)}_{j+1}\right] + [\mathbf{C}_j]\left[\mathbf{T}^{(i)}_{j+1}\right] = [\dot{\mathbf{B}}_{\rm ex}] \tag{18}$$

where the subscript $j(j = 1, 2, \ldots)$ represents the number of iteration steps; $[\mathbf{C}_j] = [\mathbf{C}(\sigma_{s,j})]$; $\sigma_{s,j} = J_j/E_j$, and J_j and E_j are the magnitudes of $\mathbf{J}_j$ and $\mathbf{E}_j$, respectively. The initial conductivities $\sigma_{s,1}$ at the first step of iteration with symbol j are chosen by the sufficiently big values in the whole superconductor.

4) *Numerical integration of* (18). At each step j, the Crank–Nicolson-θ method is employed to perform the numerical integration of (18) such that the response $[\mathbf{T}^{(i)}_{j+1}] = [\mathbf{T}^{(i)}_{j+1}(t)]$ varying with time is obtained numerically.

5) *Precision condition*. Once the iterated solutions J_{j+1} and E_{j+1} are gained from the solution of (18), the iterated value $\sigma_{s,j+1} = J_{j+1}/E_{j+1}$ is obtained at each element. Replacing the iterating values $\sigma_{s,j}$ by their corresponding iterated values $\sigma_{s,j+1}$ at all elements, and repeating the iteration process of (18), we may get the numerical solution of electromagnetic fields of the superconductor until the following condition is satisfied at all elements:

$$|\sigma_{s,j+1} - \sigma_{s,j}| < \delta_1 \tag{19}$$

Here, $0 < \delta_1 \ll 1$ is a pregiven precision. After that, we can obtain the magnetic force $F^{(i)}_{\rm em}$ of ith iteration.

Step 3) *Numerical integration of* (10). After the Newmark-β method is employed to take numerical integration of (10), we get the numerical response $z^{(i+1)}(t)$ and $\dot{z}^{(i+1)}(t)$, or the iterated solutions of $z(t)$ and $\dot{z}(t)$.

Step 4) Replace the iterating solutions $z^{(i)}(t)$ and $\dot{z}^{(i)}(t)$ by the iterated solutions $z^{(i+1)}(t)$ and $\dot{z}^{(i+1)}(t)$, respectively, and repeat the calculations of Steps 1–3 until the following precision condition is held:

$$\left|z^{(i+1)}(t) - z^{(i)}(t)\right| < \delta_2 \tag{20}$$

Here, $0 < \delta_2 << 1$ is a prescribed tolerance.

IV. RESULTS AND DISCUSSION

Based on the introduced numerical code, we display some results of numerical tests and case studies to the levitation systems considered. The geometric and material parameters used in the calculations are listed in Tables I and II, some of which are the same as those given by Yoshida *et al.* [19].

The first examination of the numerical code is to simulate the measurement data of time-varying magnetic force of the levitation system [19]. In this experiment, the levitated PM is driven to move to the fixed superconductor from 25 to 0.5 mm in gap at a specified constant speed of about 15 mm/s, and then stayed at the levitation gap 0.5 mm. Fig. 3 displays time-variation of the magnetic force obtained from both the experimental measurement and the simulation here. From this figure, one sees that after the magnetic force approaches to a maximum value or peak, the predictions on the basis of the flux flow and creep model are closer to the experimental data than those based on

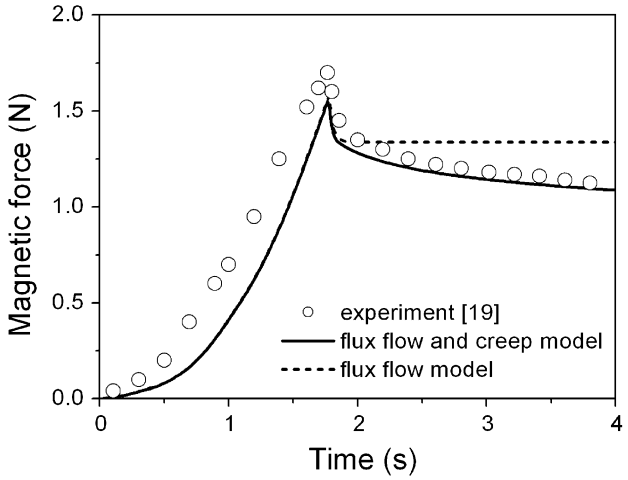

Fig. 3. Comparison of simulations with experimental data of magnetic force varying with time. The parameters of $J_c = 1.5 \times 10^7$ A/m^2, $U_0 = 92$ meV, $\rho_f = 7.62 \times 10^{-10}$ Ωm, and others listed in Table I are employed.

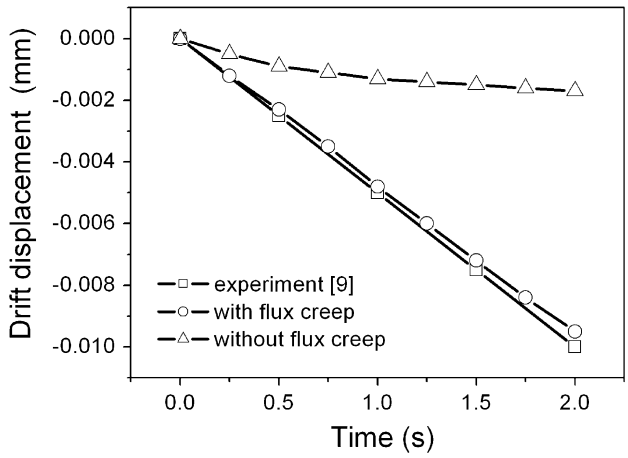

Fig. 4. Comparison of simulations with experimental data of drift displacement of vibration center of the levitation system. The parameters of the system are listed in Table II.

the flux flow model. At the stage before the peak, almost no difference between the predictions from these two models is found, but there is a difference between the predictions and the experimental data. In the practical experiment, the accelerating and decelerating periods are needed to realize the motion of PM. Once we consider the accelerating/decelerating period of 0.01 and 0.05 s in the theoretical simulation with the flux flow and creep model, respectively, the predictions exhibit the same as that shown in Fig. 3 except for a small drop of the peak. When we increase the moving velocity of PM in the simulation for example, it is found that the peak in the prediction moves notably toward the left and the value of the peak has a slight change so the prediction of magnetic force before the peak increases too. In this case, we guess that one possible reason for generating this difference is that some physical parameters, e.g., the critical current density J_c and the flow resistivity ρ_f, of HTSC employed in simulation are not accurate since they are not accurately measured.

The second examination of the numerical code is to predict the experimental phenomenon of downward drift of vibration center of LB in the levitation system [9]. In this experiment, a harmonic excitation of vertical displacement, $A\sin(2\pi f_a t)$, is applied. Here, the amplitude and frequency are taken as $A = 50\,\mu$m and $f_a = 50$ Hz, respectively. At the same time, zero deviations of initial displacement and velocity related to the equilibrium position of the system were set in the experiment. In the literature [9], some parameters were given by their regions rather than fixed values. Here, we take them in their regions with some determinant values that are listed in Table II. Fig. 4 plots the vibration center of the LB varying with time, which tells us that the predictions from the flux flow and creep model are well in agreement with their measurement data, but those from the flux flow model are not.

From the above two examinations of the numerical code to the levitation system, we find that this code enables us to simulate the magnetic force and the dynamic behavior of relevant levitation systems, and that the predictions to the systems on the basis of the flux flow and creep model are more accurate than ones from the flux flow model. From Table II, one can also find that the experimental parameters including the scale of superconductor, critical current density, and residual field of PM are too either small or low compared with practical applications. Since the dynamic behavior of the levitation system is dependent on the parameters, we give some case studies with the parameters taken in the range of practical applications.

At the following simulations of magnetic force and dynamic behavior of the levitation system, the parameters in Table I are employed if they are not specified separately. Here, the mass of PM is 93.8 g, and the mass of the additional load may be changed to realize a given gap. Following [17], the air-damping coefficient is taken as 0.5 Ns/m for example.

In order to obtain a theoretical initial condition of dynamic response of this levitation system, the typical magnetic force-gap curves in field cooling haven been shown in Fig. 5, in which Fig. 5(a) exhibits an approach–depart process (initial cooling height 15 mm) and Fig. 5(b) a depart–approach process (initial cooling height 0.5 mm). Every magnetic force-gap curve contains one major and several minor loops, and the magnetic stiffness [only in Fig. 5(a)]. These important results were measured earlier by Moon [3], and then by Hull [6], who discussed the highly hysteretic characteristic of magnetic force-gap relation and magnetic stiffness. In general, magnetic stiffness is related to the slope of the minor loops rather than the slope of the major hysteresis loop [3]. So, as shown in Fig. 5(a), the magnetic stiffness is introduced as [3], [6]

$$k = -\frac{\Delta f}{\Delta z} \tag{21}$$

where Δz indicates minor loop traverse (following [22]); and Δf represents the differential value of end points relevant to the minor loop traverse. In fact, there is a slight influence of the minor loop traverse on the magnetic stiffness [22], whereas the minor loop traverse Δz is taken as 1 mm for simplicity here. Also, all the points on a minor loop were fitted with a straight line to find the slope of each minor loop, which in turn provides the stiffness for a particular Δz. In general, at the point on a major loop, the slope of the minor loop is not the same as that

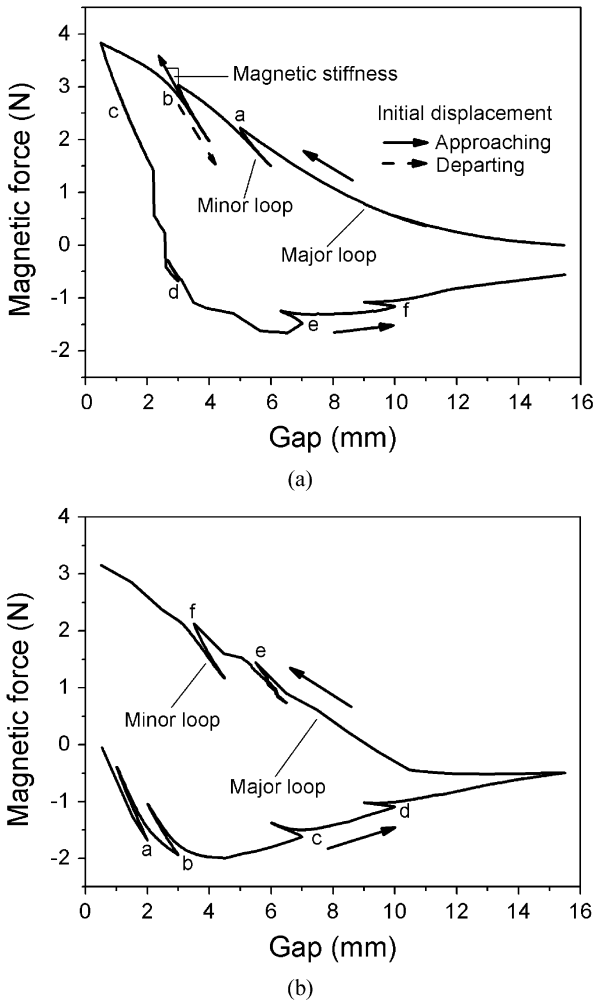

Fig. 5. Hysteresis loop of magnetic force-gap and magnetic stiffness in field cooling; several minor loops for different points on major loop. (a) Approach–depart process: the initial cooling gap is 15 mm; the levitation gaps of point $a, b, c, d, e,$ and f are 5, 3, 2, 3, 7, and 10 mm, respectively. (b) Depart–approach process: the initial cooling gap is 0.5 mm; the suspension gaps of point $a, b, c, d, e,$ and f are 2, 3, 7, 10, 5, and 3 mm, respectively.

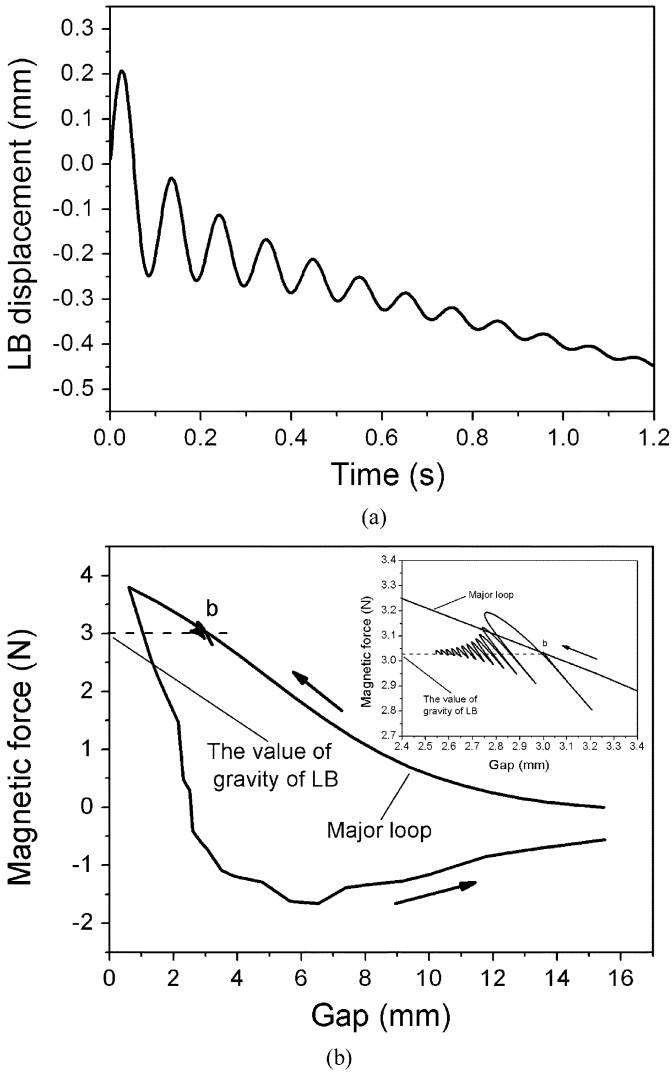

Fig. 6. Characteristic curve of free vibration drift of LB located at the point b in Fig. 5(a). (a) Dynamic response; (b) magnetic force-gap relation.

of the major one, e.g., the points a, b in Fig. 5(a) and the points a, b in Fig. 5(b), while at other points the slope of the minor loop is almost the same as that of the major one, e.g., the point c in Fig. 5(a). The necessary condition of stable levitation is generally considered as [3], [6]

$$k > 0. \tag{22}$$

According to this condition, it can be concluded that, in Fig. 5(a), the points $a, b, c,$ and d are possibly stable, while the points e and f are certainly unstable; in Fig. 5(b), points $a, b, e,$ and f are possibly stable, while the points c and d are certainly unstable.

The key results of this research are shown in Figs. 6–8, in which the characteristic curves of free vibration drift of the LB, including the dynamic response and the magnetic force-gap relation under free vibration, are plotted. Once the LB statically levitated at point b in Fig. 5(a) is applied, a given initial disturbance (e.g., the initial velocity 15 mm/s in this paper), it begins to vibrate freely. The dynamic response of this LB and the magnetic force-gap relation varying with time are, respectively, shown in Fig. 6(a) and (b). Obviously, as shown in Fig. 6(a), the vibration center drifts downwards, i.e., the levitation gap decreases, and similar to a damped vibration, the amplitude of dynamic response decreases with time little by little. We guess that flux motion in superconductors, which makes the energy of this levitation system decrease, is one of main reasons. All of the above characteristics are indirectly shown in Fig. 6(b). In the process of free vibrating of the LB, the magnetic force on the PM (or HTSC) varies always around a certain value, i.e., the value of gravity of the LB [indicated by the short dash in Fig. 6(b)], and the gap decreases with time [shown clearly in the insertion picture of the Fig. 6(b)]. These similar results have ever been obtained theoretically by Hikihara *et al.* [10]. However, the mathematic model in his research is very difficult to reflect the physical nature of levitation drift of high-T_c superconducting levitation systems due to simple and approximate equivalence. From these simulation results, it is concluded that, the equilibrium position of the LB in high-T_c superconducting levitation systems exists not a space point, but a continuous range. This

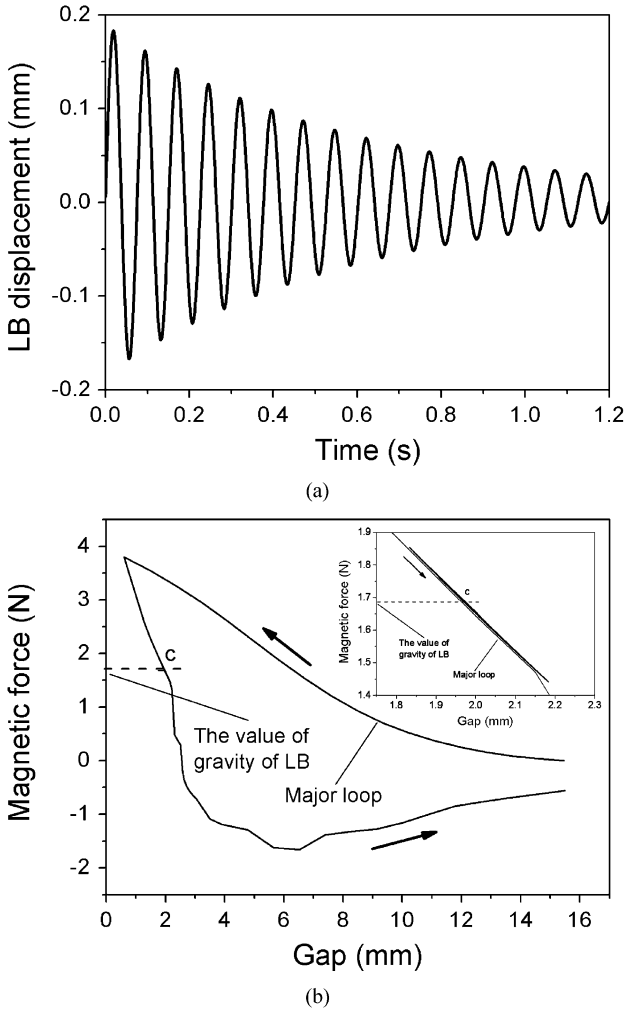

Fig. 7. Characteristic curve of free vibration drift of LB located at point c in Fig. 5(a). (a) Dynamic response; (b) magnetic force-gap relation.

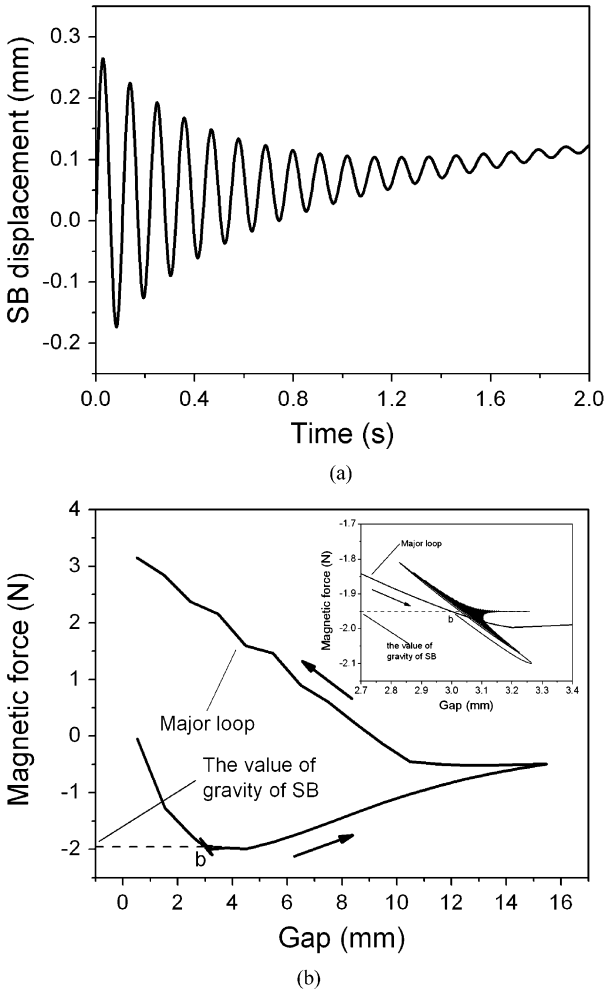

Fig. 8. Characteristic curve of free vibration drift of SB located at point b in Fig. 5(b). (a) Dynamic response; (b) magnetic force-gap relation.

problem has ever been studied experimentally earlier by Brandt [13], and recently by Navau *et al.* [14], but they are only from the aspect of static cases. In addition, damped vibration of the LB can be also found indirectly from Fig. 6(b). The similar results at point c in Fig. 5(a) are shown in Fig. 7. Compared with those in Fig. 6, the great difference is that the vibration center of the LB does not almost drift. In fact, the dynamic characteristic of the LB is closely related to its minor loop on the major loop: if the slope of the minor loop is not tangential to the major at a given point, the LB located at this point can *possibly* drift ("possibly" means that it is one of the necessary conditions of drift. In addition, there are other influences, e.g., critical current density J_c, also on drift, which will be studied in the next paper); if the slop of the minor loop is tangential to the major at a given point, so the LB located at this point can impossibly drift. According to this criterion, one can draw a conclusion that the LB at point b drifts, while at point c does not almost drift.

From the magnetic force-gap relation of the other physical process shown in Fig. 5(b), we can also find that the magnetic force is highly hysteretic, and furthermore, in some gaps, its value changes to be negative; in other words, the repulsive magnetic force changes to be an attractive one. If this attractive magnetic force is large enough, an SB can be suspended stably in the Earth's surface gravitational field. In this case, the levitation structure shown in Fig. 1 (see in the previous paper) can be changed to the suspension one, in which the PM in connection with an additional load is called as the SB. Similarly, applied by an initial disturbance, the SB located at point b in Fig. 5(b) begins to freely vibrate, and its dynamic response and magnetic force-gap relation are simulated as shown in Figs. 8(a) and (b), respectively. Compared with results in Figs. 6 and 7, the great difference is that the vibration center of the SB drifts upwards little by little. It means that the SB suspended below the HTSC departs from the HTSC, or the suspension gap increases with time, in the process of free vibrating of the SB. Even in accord with the discussion above, the slope of the minor loop at point b in Fig. 5(b) is not tangential to the major loop at this point. In addition, other characteristics such as the continuous equilibrium position of SB and damped vibration as shown in Fig. 6 can also be observed.

V. Conclusion

Based on studying drift of LB/SB in high-T_c superconducting levitation systems under vibration, a criterion on the magnetic

force-gap relation for the gap varying with time has been presented in this paper. According to the suggested criterion, it can be concluded that dynamic behavior of the LB/SB is closely related to its minor loop at a given point on the major loop. The LB/SB located at a given point will *possibly* drift if the slope of the minor loop is not tangential to the major loop at this point: the LB/SB will *possibly* drift downwards (i.e., the levitation gap will decrease) if it is located at the approaching part of the major loop, and it will *possibly* drift upwards (i.e., the suspension gap will increase) if it is located at the departing part (also, on which magnetic stiffness $k > 0$) of the major loop.

ACKNOWLEDGMENT

The authors would like to thank the reviewers for their valuable suggestions in the revisions.

REFERENCES

[1] E. H. Brandt, "Levitation in physics," *Science*, vol. 243, pp. 349–355, 1989.
[2] T. H. Johansen, Z. J. Yang, H. Bratsberg, G. Helgesen, and A. T. Skjeltorp, "Lateral force on a magnet placed above planar $YBa_2Cu_3O_x$ superconductor," *Appl. Phys. Lett.*, vol. 58, no. 2, pp. 179–181, 1991.
[3] F. C. Moon, *Superconducting Levitation*. New York: Wiley, 1994.
[4] J. S. Wang, S. Y. Wang, Y. W. Zeng, H. Y. Huang, F. Luo, Z. P. Xu, Q. X. Tang, G. B. Lin, C. F. Zhang, R. Z. You, G. M. Zhao, D. G. Zhu, S. H. Wang, H. Jiang, M. Zhu, C. Y. Deng, P. F. Hu, C. Y. Li, F. Liu, J. S. Lian, X. R. Wang, L. H. Wang, X. M. Shen, and X. G. Dong, "The first man-loading high temperature superconducting maglev test vehicle in the world," *Physica C*, vol. 378–381, pp. 809–814, 2002.
[5] J. S. Wang, S. Y. Wang, Y. W. Zeng, C. Y. Deng, Z. Y. Ren, and X. R. Wang, "The present status of high temperature superconducting maglev vehicle in China," *Supercond. Sci. Technol.*, vol. 18, pp. S215–S218, 2005.
[6] J. R. Hull, "Topic Review: Superconducting bearing," *Supercond. Sci. Technol.*, vol. 13, pp. R1–R15, 2000.
[7] S. O. Siems and W.-R. Canders, "Advances in the design of superconducting magnetic bearings for static and dynamic applications," *Supercond. Sci. Technol.*, vol. 18, pp. S86–S89, 2005.
[8] V. V. Nemoshkalenko, E. H. Brandt, A. A. Kordyuk, and B. G. Nikitin, "Dynamics of a permanent magnet levitating above a high-T_c superconductor," *Physica C*, vol. 170, pp. 481–483, 1990.
[9] A. N. Terentiev and A. A. Kuznetsov, "Drift of levitated YBCO superconductor induced by both a variable magnetic field and a vibration," *Physica C*, vol. 195, pp. 41–46, 1992.
[10] T. Hikihara and F. C. Moon, "Levitation drift of a magnet supported by a high-T_c superconductor under vibration," *Physica C*, vol. 250, pp. 121–127, 1995.
[11] T. A. Coombs and A. M. Campbell, "Gap decay in superconducting magnetic bearings under the influence of vibrations," *Physica C*, vol. 256, pp. 298–302, 1996.
[12] X.-J. Zheng, X.-F. Gou, and Y.-H. Zhou, "Influence of flux creep on dynamic behavior of magnetic levitation systems with a high-T_c superconductor," *IEEE Trans. Appl. Supercond.*, vol. 15, no. 3, pp. 3856–3863, Sep. 2005.
[13] E. H. Brandt, "Friction in levitated superconductors," *Appl. Phys. Lett.*, vol. 53, pp. 1554–1556, 1988.
[14] C. Navau, A. Sanchez, E. Pardo, and D.-X. Chen, "Equilibrium positions due to different cooling processes in superconducting levitation systems," *Supercond. Sci. Technol.*, vol. 17, pp. 828–832, 2004.
[15] I.-G. Chen, J. Liu, R. Weinstein, and K. Lau, "Characterization of $YBa_2Cu_3O_7$ including critical current density J_c, by trapped magnetic field," *J. Appl. Phys.*, vol. 72, pp. 1013–1020, 1992.
[16] Y. Yoshida, M. Uesaka, and K. Miya, "Magnetic field and force analysis of high T_c superconductor with flux flow and creep," *IEEE Trans. Magn.*, vol. 30, no. 5, pt. 2, pp. 3503–3506, Sep. 1994.
[17] T. Sugiura and H. Fujimori, "Mechanical resonance characteristics of a high-T_c superconducting levitation system," *IEEE Trans. Magn.*, vol. 32, no. 3, pt. 1, pp. 1066–1069, May 1996.
[18] T. Sugiura, M. Tashiro, Y. Uematsu, and M. Yoshizawa, "Mechanical stability of a high-T_c superconducting levitation system," *IEEE Trans. Appl. Supercond.*, vol. 7, no. 2, pp. 386–389, Jun. 1997.
[19] Y. Yoshida, M. Uesaka, and K. Miya, "Evaluation of dynamic magnetic force of high-T_c superconductor with flux flow and creep," *Int. J. Appl. Electromagn. Mater.*, vol. 5, pp. 83–89, 1994.
[20] M. Uesaka, Y. Yoshida, N. Takeda, and K. Miya, "Experimental and numerical analysis of three-dimensional high-T_c superconducting levitation," *Int. J. Appl. Electromagn. Mater.*, vol. 4, pp. 13–25, 1993.
[21] Y. H. Zhou and X. J. Zheng, *Mechanics of Electromagnetic Solid Structures*. Beijing, China: Science Press, 1999, (in Chinese).
[22] J. R. Hull and A. Cansiz, "Vertical and lateral forces between a permanent magnet and a high-temperature superconductor," *J. Appl. Phys.*, vol. 86, pp. 6396–6404, 1999.

Xiao-Fan Gou received the Ph.D. degree in superconductivity from Lanzhou University, Lanzhou, Gansu, China, in 2004.

In 2006, he was appointed an Associate Professor in the Department of Engineering Mechanics, Hohai University, Nanjing, Jiangsu, China. Now his research interests are in the numerical analysis of electromagnetic phenomena in superconductors, including the application of superconductors to levitation.

Xiao-Jing Zheng received the Masters Degree in Engineering Science from Huazhong University of Science and Technology, Wuhan, Hubei, China, in 1984, and the Ph.D. degree from Lanzhou University, Lanzhou, Gansu, China, in 1987.

Since 1991, she has been a Professor in the Department of Mechanics, Lanzhou University, Gansu, China. Her research interests include analysis of mechanics of multifield coupling, electro-magneto-solid mechanics, and electrification mechanism of aeolian sand grains, etc. She has published about 140 papers and two text books in her research areas.

You-He Zhou received the Masters Degree in Engineering Science from Huazhong University of Science and Technology, Wuhan, Hubei, China, in 1984, and the Ph.D. degree from Lanzhou University, Lanzhou, Gansu, China, in 1989.

He was appointed a Professor of the Department of Mechanics, Lanzhou University, Lanzhou, China, in 1996. His research interests include dynamic analysis, electro-magneto-solid mechanics, and dynamic control of smart structures, etc. He has published about 160 papers and one textbook in his research areas.